UCRL-JC-123070
PREPRINT

Characterization of Third-Harmonic Target Plan and Irradiance on the National Ignition Facility Beamlet Demonstration Project

Paul J. Wegner, Bruno M. Van Wonterghem, Shamasunder N. Dixit, Mark A. Henesian, Charles E. Barker, Calvin E. Thompson, Lynn G. Seppala and John A. Caird

This paper was prepared for submittal to the
12th Topical Meeting on the Technology of Fusion Energy
Reno, NV
June 16-20, 1996

April 25, 1997

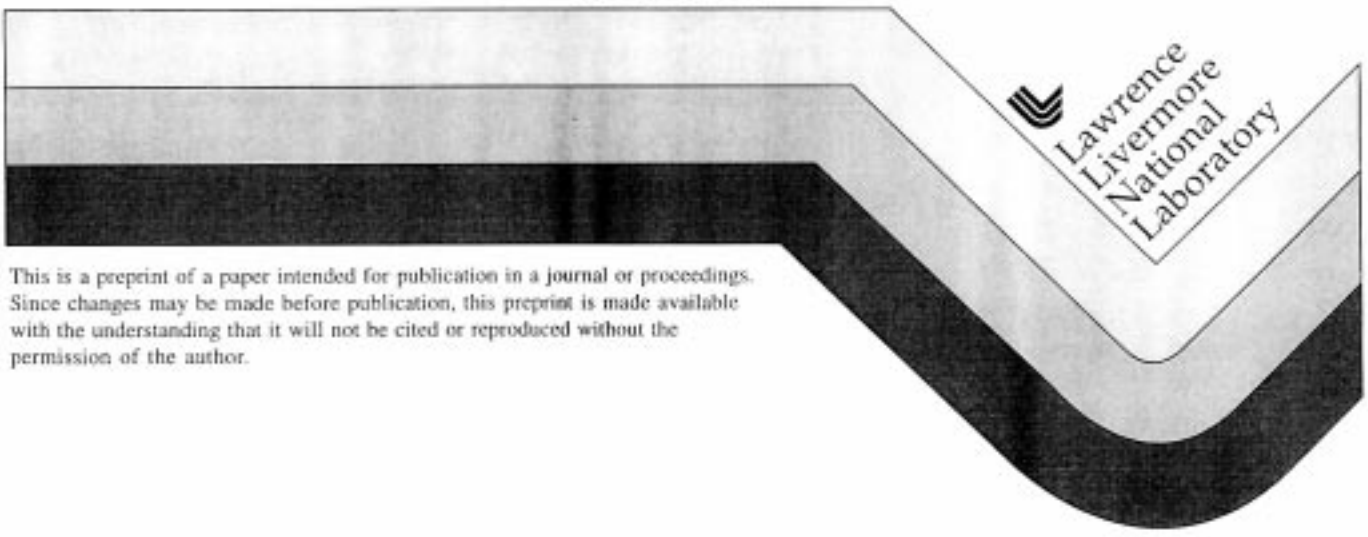

CHARACTERIZATION OF THIRD-HARMONIC TARGET PLANE IRRADIANCE ON THE NATIONAL IGNITION FACILITY BEAMLET DEMONSTRATION PROJECT

Paul J. Wegner, Bruno M. VanWonterghem, Shamasunder N. Dixit, Mark. A. Henesian, Charles E. Barker, Calvin. E. Thompson, Lynn. G. Seppala and John A. Caird

Lawrence Livermore National Laboratory
PO Box 808, L- 487
Livermore, CA 94550
(510) 423-2483

ABSTRACT

The Beamlet laser is a single-aperture prototype for the National Ignition Facility (NIF). We have recently installed and activated a 55 m^3 vacuum vessel and associated diagnostic package at the output of the Beamlet that we are using to characterize target plane irradiance at high power. Measurements obtained both with and without a kinoform diffractive optic are reported. Dependences on critical laser parameters including output power, spatial filtering, and wavefront correction are discussed and compared with simulations.

I. INTRODUCTION

ICF target designs for the NIF demand high-quality beams from the laser driver. A typical indirect drive target for ICF consists of a fuel capsule centered in a can-shaped hohlraum; beams from the driver enter the target through laser entrance holes (LEH's) located on each end of the can.[1] The LEH's are designed to be small- on the order of 3 mm or less- to maintain a uniform irradiation environment for the capsule and to minimize radiation transport losses from the hohlraum. Nevertheless, plasma blow-off from the edges of the LEH must not clip the beams, even at late times in the drive pulse, therefore the beams must be focused to a diameter that is substantially smaller than that of the LEH. A further requirement is that the laser irradiance on the walls of the hohlraum be smooth and devoid of hot spots that would otherwise drive plasma filamentation and stimulated scattering processes, and reduce the efficiency of the implosion.[2] Therefore, there is a need to tailor the spatial profile of the focused drive beam and apply some form of temporal smoothing. These conditions are to be met at a total drive energy of 1.8 MJ and a peak power of 500 TW, which it is estimated will produce ignition with a safety margin of two.[3] For the 192 beamlets of the NIF, this translates into an energy of 9.4 kJ and a peak power of 2.6 TW per beamlet.

In this paper we discuss measurements performed on the Beamlet Laser Facility at Livermore to characterize target plane irradiance at the power levels expected for the NIF. We compare our results to the NIF specifications, and identify the critical laser parameters impacting performance that will enable us to extrapolate these results from Beamlet to the NIF.

II. TARGET REQUIREMENTS FOR LASER IRRADIANCE

The design requirements for the NIF include the following criteria for the focused laser spot. Focal spot characteristics other than those described here have been requested by a number of NIF user groups, however the emphasis here will be on the baseline requirements for the NIF as specified in the system design requirements. The design energy of 1.8 MJ and the design power of 500 TW is to be delivered at a wavelength of 0.351 μm inside a 600-μm diameter spot (half-angle of 43μrad for the NIF 7-meter focus lens). The spot profile is to approximate an eighth-power super-Gaussian with 1/e radius of no more than 250 μm

$$I(r) \approx I_0 \exp\left[-(r/r_0)^8\right], \quad r_0 \le 250\,\mu\mathrm{m} \tag{1}$$

At a radius of 1.5 mm corresponding to the nominal size of the target LEH, the irradiance is to be less than 10^{14} W/cm^2. Beam smoothing requirements for the spot profile have not yet been tested on the Beamlet and will not be discussed in detail in this paper. The requirements call for the focal spot to be temporally smoothed using one-dimensional dispersion of

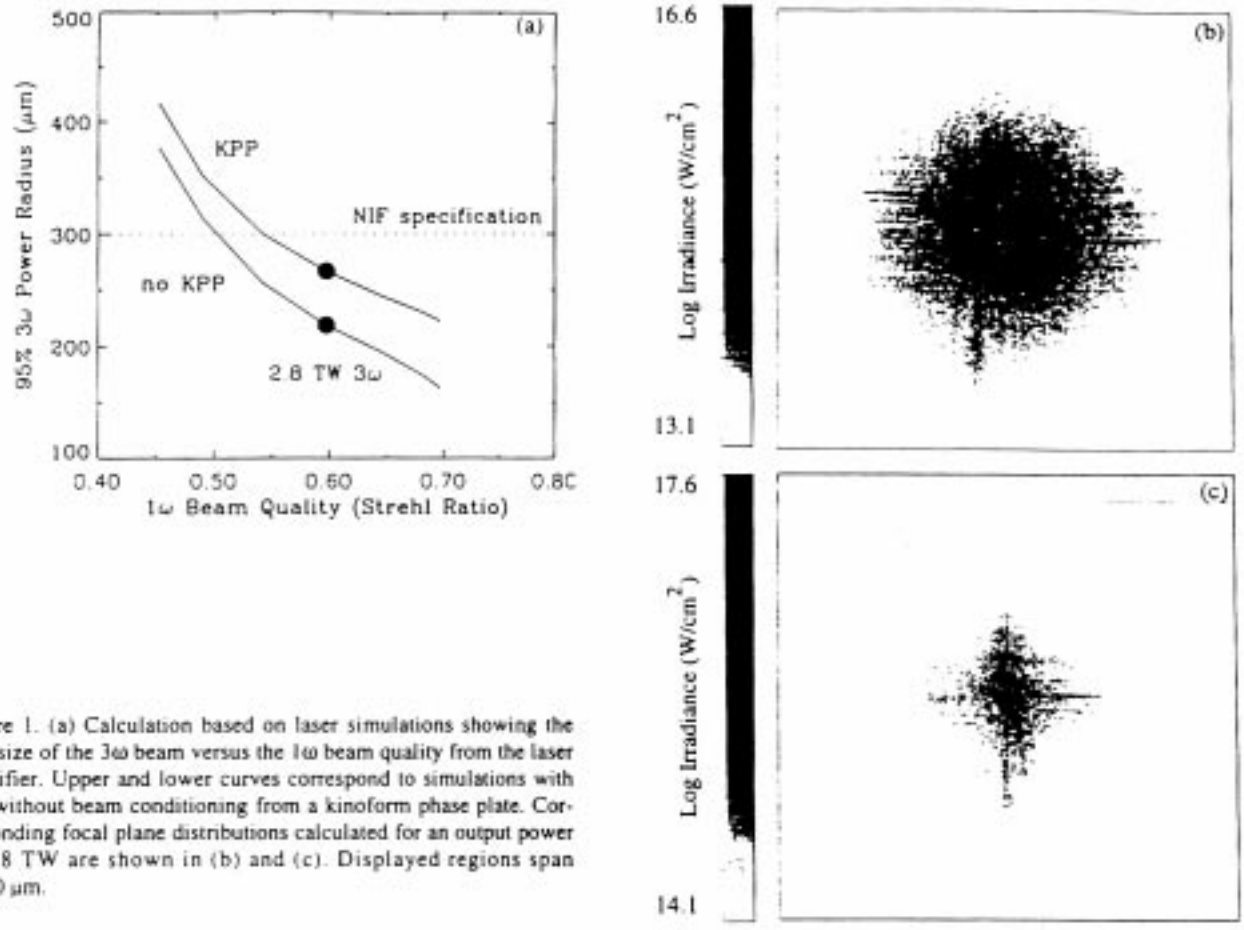

Figure 1. (a) Calculation based on laser simulations showing the spot size of the 3ω beam versus the 1ω beam quality from the laser amplifier. Upper and lower curves correspond to simulations with and without beam conditioning from a kinoform phase plate. Corresponding focal plane distributions calculated for an output power of 2.8 TW are shown in (b) and (c). Displayed regions span ± 600 μm.

3 angstroms of laser bandwidth, critically dispersed.[4]

III. LASER CONTROL PARAMETERS

Calculations indicate that the above criteria can be met provided the quality of the beam from the driver is maintained at a high level. Figure 1 shows results from full-aperture laser simulations of the Beamlet which calculate the spot size of the 0.351-μm beam (3ω) delivered to the target versus the the quality of the 1.053-μm beam (1ω) at the output of the laser amplifier. The lower curve is calculated for the case of no beam conditioning; the upper curve for the case when the 3ω beam is conditioned with a diffractive optic called a kinoform phase plate (KPP). The purpose of the KPP is to modify the aberrated focal spot produced by the laser to produce a more homogeneous irradiance distribution in the form of a speckle field with a spatial envelope that closely approximates the required eighth-power super Gaussian.[5] The price paid for the improvement in distribution is an increase in the spot size; nevertheless the simulations indicate that at an output power of 2.8 TW (3ω) we should be able to meet the NIF specification of 2.6 TW inside of 600 μm.

There are several laser performance issues that affect beam quality and determine whether we can in fact meet the NIF specifications. First, there are low-frequency thermally induced wavefront distortions originating in the laser amplifier that must be corrected with a deformable mirror.[6] Figure 2a shows a calculation of the wavefront at the output of the Beamlet for the case of no wavefront correction; the ± 1 wave of distortion shown in the figure is caused by pump-induced steering effects in the amplifier slabs. When correction is applied with a deformable mirror having the surface figure shown in Figure 2b, the output wavefront is calculated to be nominally flat and the 1ω Strehl ratio is increased from 0.1 to > 0.7. The mirror in these simulations is a model of the 39-actuator device currently in use on the Beamlet.[7] The angular bandwidth of the Beamlet mirror allows for the correction of

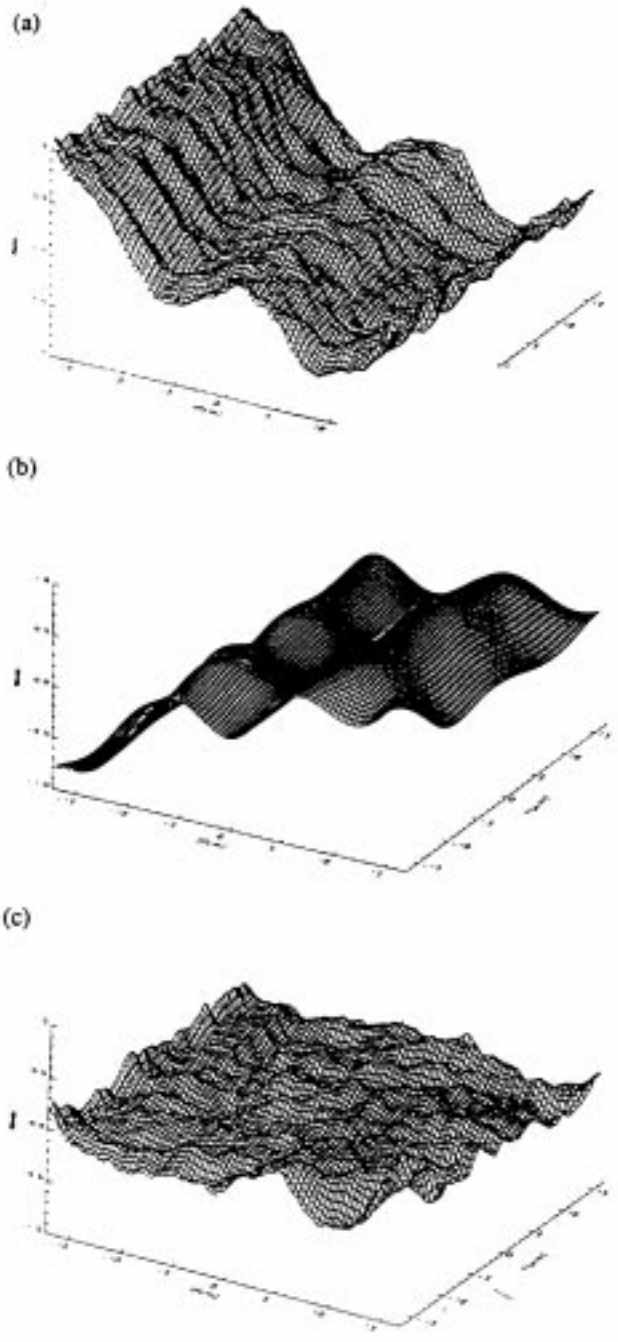

Figure 2. Simulations demonstrating the correction of long-scalelength wavefront distortions with a deformable mirror. (a) Pump induced wavefront distortions reduce the output 1ω Strehl ratio to < 0.12. (b) Surface figure of 39-actuator deformable mirror for wavefront correction. (c) Corrected low-power output wavefront with Strehl ratio of > 0.7.

wavefront errors ranging up to approximately ± 20 μrad.

Of additional concern are the amplitude and wavefront distortions in the beam that occur at frequencies exceeding the practical bandwidth of a deformable mirror. Angular bandwidth associated with high-frequency ripple can actually grow as a result of propagation instabilities in the laser. The mechanism for growth is the intensity-dependent refractive index in the laser components, a manifestation of the third-order Kerr effect, which enables a weak ripple wave co-propagating with a strong pump wave to couple and scatter a fourth wave, conjugate in angle to the ripple (see Figure 3a).[8-10] Subsequent interaction of the conjugate wave with the pump generates another ripple wave, and so on, in a process which if left unchecked, leads ultimately to the generation of higher-order ripple modes, advanced self focussing and beam breakup.

Ripple growth poses a problem well before the beam-breakup stage because it is a direct means by which energy can be coupled into high-angle modes that focus outside of the target. In the perturbation regime, the ripple field can be shown to evolve through a given component as $\exp[\pm\Omega z]$, with Ω depending on the angle of the ripple wave according to

$$\Omega(\theta) = \frac{\theta}{\theta_m}\sqrt{2 - \left(\frac{\theta}{\theta_m}\right)^2}\,B_0, \qquad B_0 = \frac{2\pi n}{\lambda}\gamma I \tag{2}$$

Here I is the background intensity of the pump field, n is the refractive index, λ the wavelength and γ the nonlinear coefficient in the material. At the optimum ripple growth angle denoted by θ_m

$$\theta_m = \sqrt{\frac{2\gamma I}{n}} \tag{3}$$

power in the ripple mode grows as $\exp[2B]$ with $B = B_0 z$ being the familiar notation for the nonlinear phase shift incurred by the ripple wave. On systems with many components of various spacings, the actual power gain and its dependence on ripple angle can be quite complex,[11] as demonstrated by Figure 3b, which plots the calculated ripple growth spectrum for the Beamlet laser at a 3ω output power of 3.5 TW. The lower curve, corresponding to the 1ω spectrum, was generated by injecting a field with perturbative noise terms uniformly distributed in phase and amplitude into a model of the laser amplifier and calculating the gain at the output as a function of ripple angle. The large peak visible at 200 μrad reflects the tendency for the beam to break up into 5-mm cells unless this particular growth mode is suppressed;

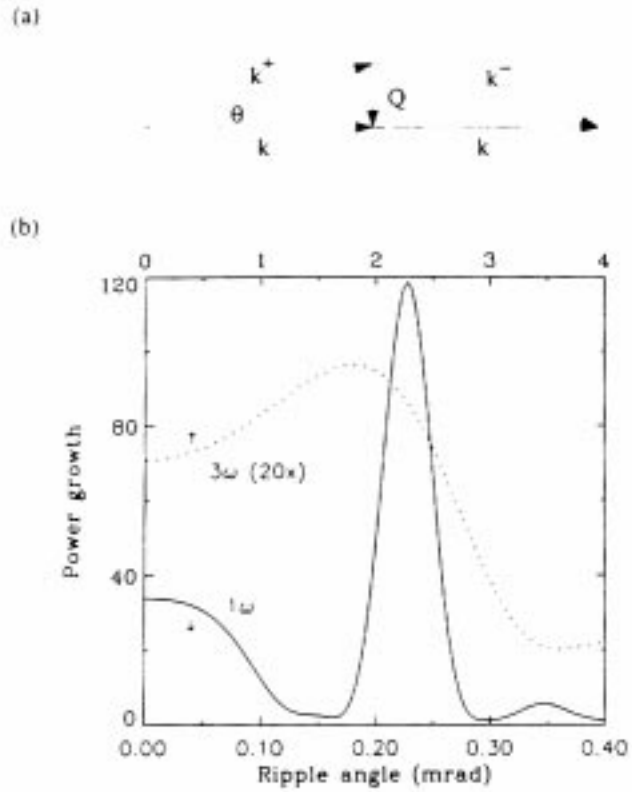

Figure 3. (a) Wave vector diagram of degenerate four-wave interaction responsible for nonlinear ripple growth in materials possessing a Kerr response Q. (b) Calculated 1ω (__) and 3ω (....) ripple growth spectra for the Beamlet laser at a 3ω output power of 3.5 TW in a 34-cm beam. 3ω curve has been scaled by a factor of 20.

thus the largest pinhole size used in the Beamlet spatial filters corresponds to a cutoff angle of ±200 μrad. The upper curve corresponds to the 3ω growth spectrum calculated for the final optics. In this case, maximum growth occurs at angles in the vicinity of 2 mrad (ripple scale lengths on the order of 100 to 200 μm) and the potential for a 5x increase in power scattered to these angles is indicated.

Controls for ripple growth are limited, but critical for the production of well- focused beams on both the Beamlet and the NIF. Optical components for these facilities must comply with stringent specifications for homogeneity and surface-finish specifically to limit the source terms for this effect. Pinhole staging in the spatial filters, and the B incurred between and after the filters are both important control parameters for the beam characterization studies discussed below.

IV. BEAMLET FOCAL PLANE DIAGNOSTICS

The Beamlet laser is a single-aperture prototype of the NIF design that was built to demonstrate the laser science and technology of the NIF architecture.[12] It incorporates a four-pass cavity containing eleven Nd:Phosphate glass amplifier slabs, a 37-cm aperture plasma-electrode Pockels cell/polarizer switch to eject the beam from the cavity, a five-slab booster amplifier, and a 37-cm aperture frequency converter comprised of a type I KDP doubler and type II KD*P tripler, which convert the 1.053-μm wavelength of the laser to the 0.351μm wavelength delivered to the target. Two 18-meter spatial filters image-relay the system and control angular bandwidth; one filter relays the cavity, and the second transports the beam from the booster amplifiers to the frequency converter. The 39-actuator deformable mirror resides in the injection optics assembly near the pinhole plane of the cavity filter.

For characterizing the irradiance in the target plane we recently installed a 55 m^3 vacuum vessel and associated diagnostic package at the output of the Beamlet, as shown in Figure 4. A square fused silica lens of 7-meter focal length forms a vacuum barrier for the vessel and produces a 3ω focus at a plane equivalent to the target location on the NIF. An off-axis lens design, per the original NIF baseline, yields an equivalent wedge angle of 4.5° which we use to angularly disperse the 3ω beam from the 1ω and 2ω (0.528 μm wavelength) radiation left over from the frequency conversion process. Provisions exist for installing a debris shield or a KPP immediately downstream of the lens when required. The focus at the target plane is imaged and attenuated by a 1-meter aperture telescope housed inside the vessel. The telescope is comprised of three uncoated spherical mirrors fabricated from fused silica and configured to form an eccentric portion of a centered optical system, as illustrated in Figure 4b. One of the principle advantages of this design is its large working distance which makes it possible to expand the post focus beam up to a size of 60 cm and thus reduce the threat of damage to the primary mirror. In addition, the design provides an unobscured aperture and is afocal, meaning that planes in the vicinity of the target plane are imaged with near-constant magnification. Auxiliary optics downstream of the telescope feed an extensive suite of energy/power detectors and imaging sensors.

The primary energy diagnostic is a full-aperture calorimeter located in the vessel near a relay plane of the final focus lens, which measures the total energy in the first, second and third harmonic wavelengths. Energy detectors for the individual wavelengths are calibrated by reference to this calorimeter. Additional detectors measure the 3ω energy in the target plane out to a radius of 20 mm (± 3 mrad), and the

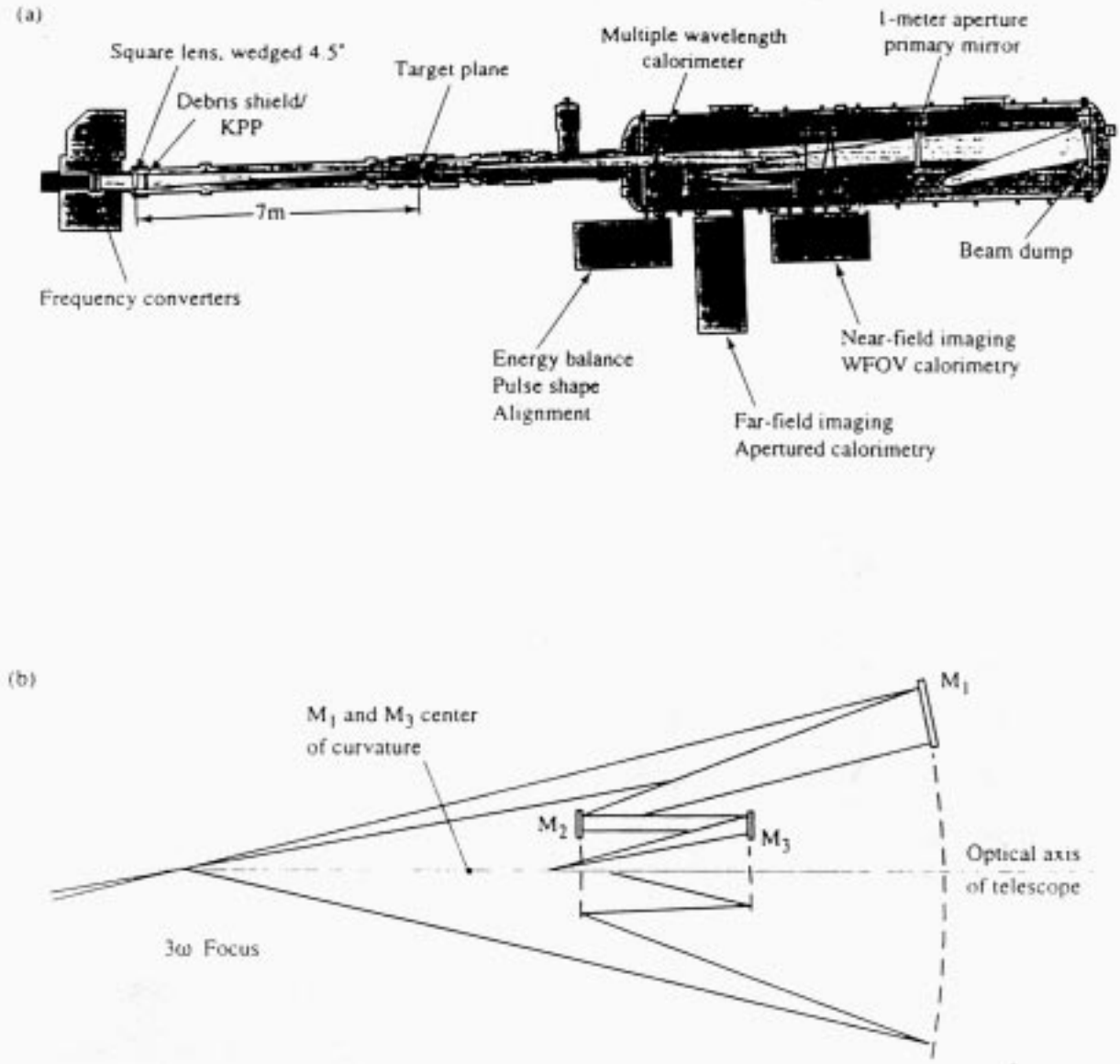

Figure 4 (a) Layout of the Beamlet focal plane diagnostics. (b) Detail showing the arrangement and optical alignment of the post focus telescope mirrors.

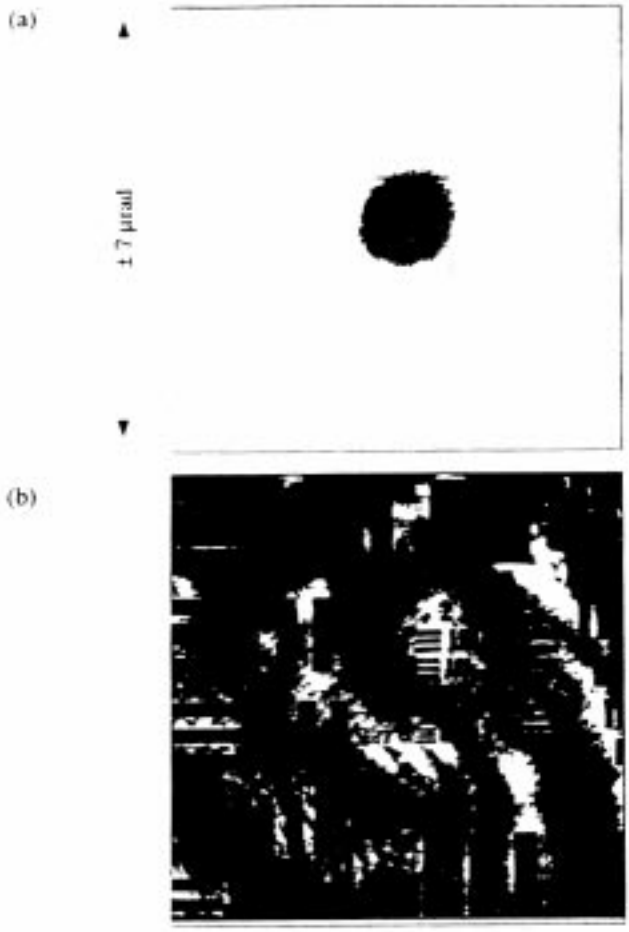

Figure 5. (a) Image of a point source situated at the target plane. 81.5% of the energy is within a spot size equal to 1.6 times the diffraction limit. (b) Image of a backlit test target located at the final focus lens, demonstrating 70 μm resolution.

fraction of this energy that passes through an aperture equivalent to the 3 mm LEH. Pulse shape is measured with a 4-ps resolution streak camera.

Imaging sensors include two target plane cameras with ±100 and ±300 μrad fields of view, a multiple image camera which views several planes spaced by 4 mm about the target plane, and two nearfield cameras which measure both large scale (> 1 mm) and fine scale (< 100 μm) beam structure at the final focus lens. Target-plane imaging is accomplished with near-diffraction limited resolution, as demonstrated by Figure 5, which shows the image of a 2ω fiber optic point source (9 μm diameter) situated at the 3ω target plane. The measurement was performed at the second harmonic because of the irradiance levels needed to overcome the losses of the uncoated telescope mirrors. Nearfield imaging capability has also been quantified. Figure 5b is an image of a resolution test target situated at the final focus lens demonstrating a resolving power of better than 14 lines per mm. This camera has only recently been activated and will be used to characterize the growth of high-frequency 3ω ripple in the final focusing optics.

V. MEASUREMENTS AND ANALYSIS

The tests we are currently conducting on the Beamlet are designed to evaluate beam quality during the most stressful period of the ICF drive pulse. The baseline ICF requirements for the NIF call for a 20 ns duration pulse with a 50x increase in power from front to back. By propagating short 200 ps duration pulses through the laser under conditions equivalent to those expected at the peak of the drive pulse we are able to obtain a "snap-shot" of beam quality that would otherwise be masked by integration effects. To simulate the conditions of reduced gain and increased B integral seen by photons at the peak of the long saturating pulse we conducted the majority of these tests with the booster amplifiers turned off.

Measurements of nearfield beam quality at high power show the irradiance distribution to be spatially uniform. Figure 6 is a CCD image of a 1.9 TW 3ω beam obtained under near red-line conditions: ΔB's of 1.0 and 1.5 radians in the cavity and booster sections respectively, with ± 200 μrad pinholes installed in the cavity and transport spatial filters. Restricting analysis of the irradiance distribution to the central 31-cm portion of the beam (to omit edge effects) reveals

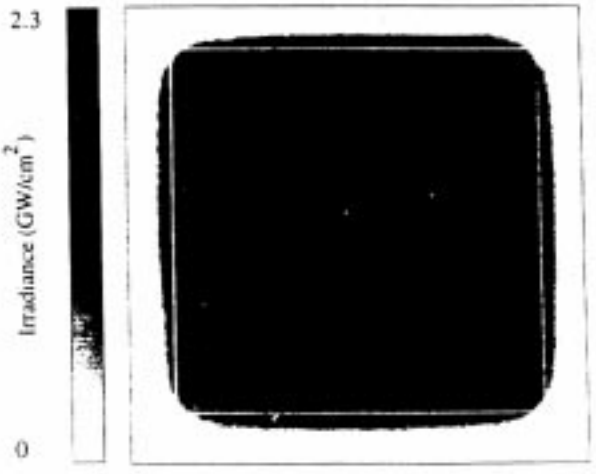

Figure 6. 1.9 TW 3ω beam at the input to the final focus lens imaged with a 1-mm resolution CCD camera. 31-cm subregion analyzed for irradiance statistics is highlighted.

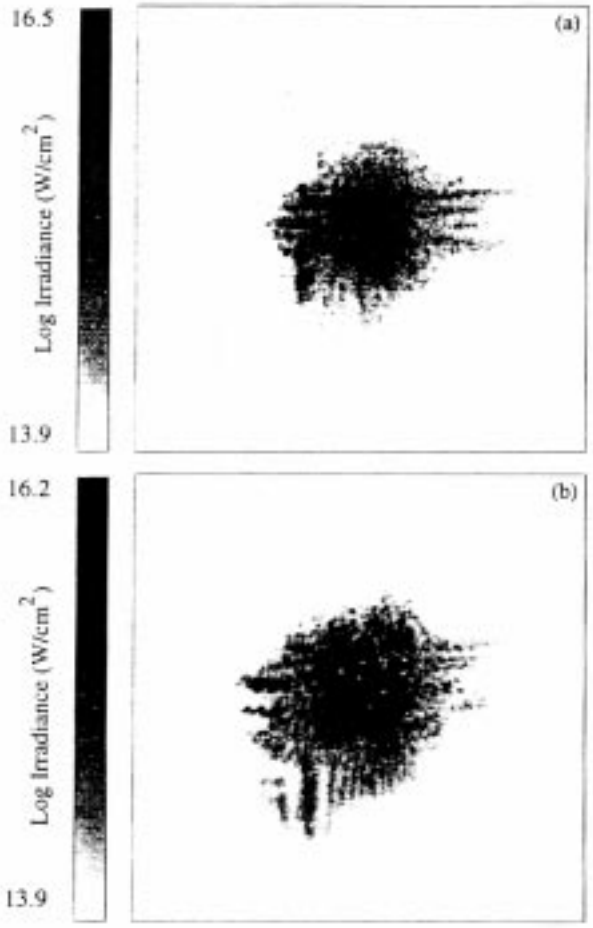

Figure 7. (a) 2.4 TW 3ω focal spot measured without the KPP. (b) Subsequent 2.1 TW 3ω focal spot showing increased distortion from thermally-induced wavefront aberrations in the amplifiers. Displayed regions span ± 600 μm.

a contrast, defined as the ratio of the standard deviation to the mean, of 0.11, with a peak to mean modulation of better than 1.35 to 1. Better compensation for spatial gain variations in the amplifiers [6] would reduce the long scale-length irradiance non-uniformities visible in the image and improve the contrast further.

Farfield measurements confirm that characteristics of the target plane irradiance on a scale length of the LEH are dominated by thermal effects in the laser amplifiers. Figure 7a shows a high-resolution CCD image of the unconditioned 3ω focal spot generated on a 2.4 TW shot. Radial integration of the image reveals that 80% of the power is contained inside a half angle of 19 μrad. This data was obtained on the first shot of the day when the amplifiers are comparatively cool. Build up of heat in the amplifiers over successive shots throughout the day generates thermal gradients and turbulence that affect beam quality, but which cannot be completely compensated for by the deformable mirror (currently the Beamlet mirror must be locked into position for a finite time period prior to each shot). Figure 7b shows this effect in the focal spot generated during the second shot of the day, in which at a reduced power of 2.1 TW, the spot size containing 80% of the power was observed to increase by over 20%. Amplifier heating is currently a problem for the Beamlet, but is not expected to be a concern for the NIF, in which active cooling is an integral part of the amplifier design.[13]

The focal spot generated with the KPP closely approaches the NIF baseline criteria for the irradiance distribution inside the LEH. Representative data obtained on a 2.1 TW shot and shown in Figure 8 reveals that 95% of the laser energy entering the LEH is contained within a 600 μm diameter spot. The 1/e radius of the spot profile measures less than 250 μm and the irradiance levels at the edge of the LEH are below 10^{14} W/cm^2. Distortions of the spot profile are evident in the form of flare-like structures extending out beyond 40 μrad. This structure contains a few percent of the energy and combined with turbulence effects, prevents the achievement of a sharply delineated distribution (see Figure 9). The origin of this structure is under investigation but it is present in the unconditioned data as well, indicating that improvements in beam quality will most likely be needed to meet the super-Gaussian profile requirement. Preliminary measurements also indicate a power-dependent increase in the level of scat-

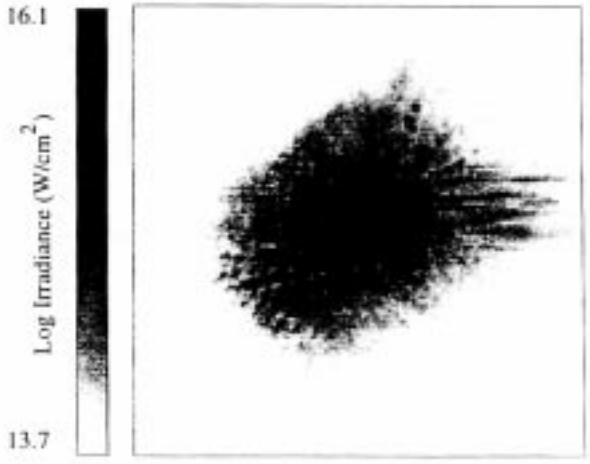

Figure 8. Measured 2.1 TW 3ω focal spot with the KPP. Displayed region spans ± 600 μm.

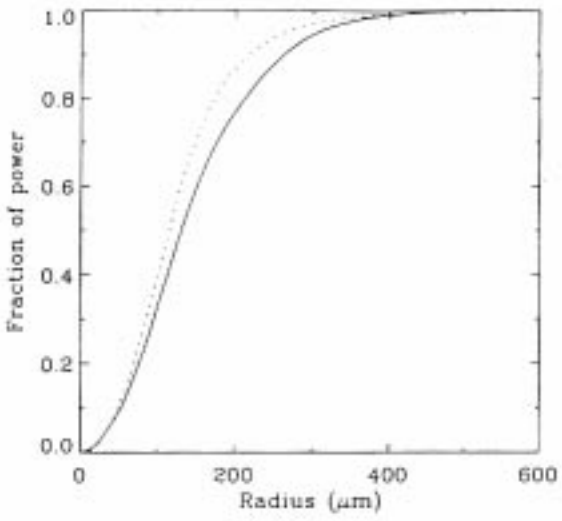

Figure 9. Radial distribution of power normalized to the total power inside the LEH for measured 2.1 TW (___) and calculated 2.8 TW (....) focal spot with beam conditioning. Model does not include turbulence effects in the amplifiers.

tered radiation lying outside of the LEH. An observed increase from ~2% at 1 TW to ~7% at 2.4 TW must be confirmed with additional measurements, but is not inconsistent with the calculation of Figure 3b.

VI. CONCLUSION

This first series of Beamlet 3ω focal spot characterization tests have come close to demonstrating the NIF requirements for laser irradiance in the target plane. Peak powers of up to 2.4 TW have been delivered through the final optics with no evidence of small-scale beam breakup or filamentation. This result has been accomplished at an aperture size that is approximately ten percent smaller than that expected for the NIF.

Several issues remain for demonstrating NIF quality focal spots on the Beamlet. Wavefront distortions generated by heat build up in the laser amplifiers cause the spot size to increase on successive shots; active cooling of the Beamlet amplifiers, and closed-loop operation of the deformable mirror up until shot time are being pursued as potential solutions to this problem. Initial measurements indicate that wide-angle scatter in the final focusing optics decreases the total amount of power delivered to the target; additional test will be conducted to confirm this effect and determine its dependence on the configuration and finish quality of the final optics. Smoothness criteria for the focal spot will be tested with the implementation of one-dimensional SSD on the Beamlet later this year.

ACKNOWLEDGMENTS

We would like to acknowledge the Beamlet operations team, whose dedicated efforts have made this work possible. C. Clay Widmayer performed the perturbation calculation of Figure 3b. The 16-level kinoform phase plate used in the tests was fabricated by Michael C. Rushford and Ian M. Thomas. This work was performed under the auspices of the U. S. Department of Energy by Lawrence Livermore National Laboratory under contract No. W-7405-ENG-48.

REFERENCES

1. J. D. Lindl, R. L. McCrory and E.M. Campbell, "Progress toward ignition and burn propagation in inertial confinement fusion," *Physics Today*, **45**, 32 (1992).

2. R. L. Berger, "Suppression of parametric instability by weakly incoherent laser beams," *Phys. Rev. Lett.*, **65**, 1207 (1990).

3. *National Ignition Facility Conceptual Design Report, Volume 2: Design Basis and Requirements*, p. 3-41, UCRL-PROP-117093 Vol 2, Livermore, CA, (1994).

4. S. Skupsky, R. W. Short, T. Kessler, R. S. Craxton, S. Letzring and J. M. Soures,"Improved laser beam uniformity using the angular distribution of frequency modulated light," *J. Appl. Phys.*, **66**, 3456 (1989).

5. S.N. Dixit, M. C. Rushford, I. M. Thomas and M. D. Perry, "Continuous contour phase plates for tailoring the focal plane irradiance profile," *Proc. Soc. Photo-Opt. Instrum. Eng.*, **2633**, 141 (1995).

6. A. C. Erlandson, M. D. Rotter, D. N. Frank and R. W. McCracken, *ICF Quarterly Report*, Lawrence Livermore National Laboratory, Livermore, CA, UCRL-LR-105821-95-1, **5**, 18 (1994).

7. J. T. Salmon, E. S. Bliss, J. L. Byrd, M. Feldman, M. A. Kartz, J. S. Toeppen, B. Van Wonterghem and S. E. Winters, "An adaptive optics system for solid-state laser systems used in inertial confinement fusion," *Proc. Soc. Photo-Opt. Instrum. Eng.*, **2633**, 105 (1995).

8. V. I. Bespalov and V. I. Talanov, "Filamentary structure of light beams in nonlinear liquids," *JETP Lett.*, **3**, 307 (1966).

9. R. L. Carman, R. Y. Chiao and P. L. Kelley, " Observation of degenrate stimulated four-photon interaction and four-wave parametric amplification," *Phys. Rev. Lett.*, **17**, 1281 (1966).

10. E. S. Bliss, D. R. Speck, J. F. Holzrichter, J. H. Erkkila and A. J. Glass,"Propagation of a high-intensity laser pulse with small-scale intensity modulation," *Appl. Phys. Lett.*, **25**, 448 (1974).

11. J. B. Trenholme, *Laser Program Annual Report*, Lawrence Livermore National Laboratory, Livermore, CA, UCRL-50021-75, 237 (1975).

12. B. M. Van Wonterghem, J. R. Murray, J. H. Campbell, D. R. Speck, C. E. Barker, I. C. Smith, D. F. Browning and W. C. Behrendt, *ICF Quarterly Report*, Lawrence Livermore National Laboratory, Livermore, CA, UCRL-LR-105821-95-1, **5**, 1 (1994).

13. M. D. Rotter, R. W. McCracken, A. C. Erlandson and D. Brown, "Thermal recovery measurements on multi-segment amplifiers," *Proc. Soc. Photo-Opt. Instrum. Eng.*, **2633**, 70 (1995).

Technical Information Department • **Lawrence Livermore National Laboratory**
University of California • Livermore, California 94551